



This paper is a part of the hereunder thematic dossier published in OGST Journal, Vol. 70, No. 5, pp. 791-902 and available online [here](#)

Cet article fait partie du dossier thématique ci-dessous publié dans la revue OGST, Vol. 70, n°5, pp. 791-902 et téléchargeable [ici](#)

DOSSIER Edited by/Sous la direction de : **D. Uzio**

IFP Energies nouvelles International Conference / Les Rencontres Scientifiques d'IFP Energies nouvelles
PHOTO4E – Photocatalysis for energy
PHOTO4E – Photocatalyse pour l'énergie

Oil & Gas Science and Technology – Rev. IFP Energies nouvelles, Vol. 70 (2015), No. 5, pp. 791-902

Copyright © 2015, IFP Energies nouvelles

- 791 > *Editorial*
M. Fontecave, A. Fécant and D. Uzio
- 799 > *Solar Production of Fuels from Water and CO₂: Perspectives and Opportunities for a Sustainable Use of Renewable Energy*
Production solaire de carburants à partir de l'eau et de CO₂ : perspectives et opportunités pour une utilisation durable de l'énergie renouvelable
R. Passalacqua, G. Centi and S. Perathoner
- 817 > *Effect of Post-Synthesis Treatments on the Properties of ZnS Nanoparticles: An Experimental and Computational Study*
Effet des traitements après-synthèse sur les propriétés de nanoparticules de ZnS : une étude expérimentale et computationnelle
E. Balantseva, B. Camino, A.M. Ferrari and G. Berlier
- 831 > *Comparative Study on The Photocatalytic Hydrogen Production from Methanol over Cu-, Pd-, Co- and Au-Loaded TiO₂*
Étude comparative de production d'hydrogène par photocatalyse à partir de méthanol et à l'aide de différentes phases actives (Cu, Pd, Co et Au) supportées sur TiO₂
P.P.C. Udani and M. Rønning
- 841 > *Photocatalytic Conversion of Carbon Dioxide Using Zn–Cu–Ga Layered Double Hydroxides Assembled with Cu Phthalocyanine: Cu in Contact with Gaseous Reactant is Needed for Methanol Generation*
Conversion photocatalytique du dioxyde de carbone par des hydroxydes doubles lamellaires de Zn–Cu–Ga promus par la phthalocyanine de Cu : nécessité du contact entre le Cu et le réactif gazeux pour la synthèse du méthanol
S. Kawamura, N. Ahmed, G. Carja and Y. Izumi
- 853 > *Recyclable PhotoFuel Cell for Use of Acidic Water as a Medium*
Cellule photocombustible recyclable pour l'utilisation d'eau acide en tant que milieu
Y. Ogura, M. Yoshida, and Y. Izumi
- 863 > *Solar Hydrogen Reaching Maturity*
L'hydrogène solaire arrive à maturité
J. Rongé, T. Bosserez, L. Huguenin, M. Dumortier, S. Haussener and J.A. Martens
- 877 > *Design of Compact Photoelectrochemical Cells for Water Splitting*
Conception de cellules photoélectrochimiques compactes pour la décomposition de l'eau
T. Bosserez, J. Rongé, J. van Humbeeck, S. Haussener and J. Martens
- 891 > *Simultaneous Production of CH₄ and H₂ from Photocatalytic Reforming of Glucose Aqueous Solution on Sulfated Pd-TiO₂ Catalysts*
Production simultanée de CH₄ et H₂ par réformage photocatalytique d'une solution aqueuse de glucose sur un catalyseur Pd-TiO₂ sulfaté
V. Vaiano, G. Iervolino, G. Sarno, D. Sannino, L. Rizzo, J.J. Murcia Mesa, M.C. Hidalgo and J.A. Navio

Recyclable PhotoFuel Cell for Use of Acidic Water as a Medium

Yuta Ogura, Mao Yoshiba and Yasuo Izumi*

Department of Chemistry, Graduate School of Science, Chiba University, Yayoi 1-33, Inage-ku, Chiba 263-8522 - Japan
e-mail: tyojuryoku@hotmail.co.jp - yubari.com@ae.auone-net.jp - yizumi@faculty.chiba-u.jp

* Corresponding author

Abstract — We reported a new PhotoFuel Cell (PFC) comprising two photocatalysts for use of acidic water as a recyclable medium. Nitrogen and oxygen flow was required in the photoanode and photocathode, respectively. In this study, we developed a gas-circulating PFC that needs no gas supply from outside. In the gas-circulating PFC, the reverse reaction of water oxidation at the anode was prevented by the gas flow of photogenerated O_2 from the anode to the cathode inside the PFC. The gas-circulating PFC accommodated an organic solvent layer over the aqueous electrolyte for the anode, and also a vent hole in the upper part of the Proton-Conducting Polymer (PCP) film. O_2 transferred from the anode electrolyte to the organic solvent due to the solubility difference between the HCl solution and organic solvent. O_2 transfer from the gas phase in the anode to that in the cathode was achieved by the vent hole in the PCP film due to the pressure difference due to the progress of the reaction. By the addition of a hexane layer to the anode of the PFC, it was demonstrated to achieve a photocurrent value of $69.7 \mu A$ per 1.3 cm^2 of photocatalysts. However, in the stability tests for more than 7 h, the small amount of remaining O_2 in the electrolyte ($2.85 \mu\text{mol L}^{-1}$) exhibited serious effects on the PFC performance. The I_{SC} , V_{OC} and P_{Max} values of the gas-circulating PFC were $29.2 \mu A$, 1.18 V and $6.10 \mu W$, that were 40%, 74% and 44%, respectively, of those for a N_2 and O_2 flow-type PFC. Apparently, photocurrents were dramatically suppressed by the reverse reaction at the photoanode in the extended tests for the gas-circulating PFC.

Résumé — Cellule photocombustible recyclable pour l'utilisation d'eau acide en tant que milieu

— Nous décrivons une nouvelle cellule photocombustible (PhotoFuel Cell, PFC) comprenant deux photocatalyseurs utilisant de l'eau acide recyclée. Un flux d'azote et d'oxygène a été nécessaire dans respectivement la photoanode et la photocathode. Dans cette étude, nous avons développé une PFC à circulation de gaz qui n'a pas besoin d'être alimentée en gaz de l'extérieur. Dans la PFC à circulation de gaz, la réaction inverse d'oxydation de l'eau à l'anode a été évitée par le flux de gaz d' O_2 photo-généré de l'anode à la cathode à l'intérieur de la PFC. La PFC à circulation de gaz présentait une couche de solvant organique au-dessus de l'électrolyte aqueux pour l'anode, et également un orifice d'aération dans la partie supérieure du film polymère conducteur de proton (Proton-Conducting Polymer, PCP). L' O_2 était transféré de l'électrolyte de l'anode au solvant organique, à cause de la différence de solubilité entre la solution d'HCl et le solvant organique. Le transfert d' O_2 de la phase gazeuse à l'anode vers celle dans la cathode a été réalisé par l'orifice d'aération dans le film PCP, du fait de la différence de pression due à la progression de la réaction. En ajoutant une couche d'hexane à l'anode de la PFC, il a été démontré que l'on atteignait une valeur de courant photo-électrique de $69,7 \mu A$ par $1,3 \text{ cm}^2$ de photocatalyseurs. Toutefois, dans les tests de stabilité, pendant plus de 7 h, la faible quantité d' O_2 restant dans l'électrolyte ($2,85 \mu\text{mol L}^{-1}$) a eu des

effets importants sur les performances de la PFC. Les valeurs I_{sc} , V_{oc} et P_{Max} de la PFC à circulation de gaz ont atteint 29,2 μA , 1,18 V, et 6,10 μW , soit 40%, 74% et 44%, respectivement de celles d'une PFC de type à flux de N_2 et d' O_2 . Apparemment, les courants photo-électriques ont été considérablement supprimés par la réaction inverse à la photoanode dans les tests prolongés pour la PFC à circulation de gaz.

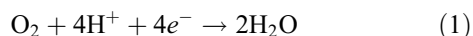
INTRODUCTION

Fossil fuels have been utilized as the essential energy source for industrialization. Industrial CO_2 emissions have led to an increase in the level of atmospheric CO_2 concentration (400 ppm), and the effects of this increase on global warming cannot be underestimated. The development of renewable energy as a replacement for fossil fuels has been slow [1, 2].

Among the renewable energies, solar energy has the greatest potential. Although the Silicon Solar Cell (Si SC) has been commercialized, the technology that can convert solar energy to electricity often needs subsidies to spread more widely [3]. Other types of SC, *e.g.* the dye-sensitized SC and compound SC [4], and Fuel Cells (FC) that use hydrogen/methanol fuel [5-8], potentially obtained using solar energy [9], have been extensively investigated. However, all the requisites (sustainability, durability and an electromotive force of 1-3 V per cell) have not been fully satisfied.

Recently, a new device was demonstrated: a PFC utilizing two photocatalysts of TiO_2 and silver(0/I)-doped TiO_2 [10] on an electrode film, both immersed in acidic solutions separated by a PCP film [11]. Platinum is not used [5-8, 12-16], and only inexpensive materials were used in the PFC for sustainability. The PFC is similar to photoelectrochemical cells (PEC) consisting of a photoanode and a photocathode to form O_2 and H_2 , respectively, from water [17, 18] and also PEC consisting of a photoanode to oxidize water [19] or organic dye fuel [20] and a photocathode to reduce protons. The PFC is different from these PEC in that the medium, water, is recycled in the cell and no fuel is needed except for natural light [21].

Although PFC enable higher electromotive force (1.8 V) [11, 21] and use only acidic water as a medium and inexpensive catalysts, PFC need a gas supply to promote surface reactions at both the anode and cathode. At the anode, O_2 gas needs to be evacuated by N_2 flow to prevent a reverse surface reaction:



On the other hand, at the cathode reactant O_2 should be supplied for the reaction (1) to proceed. Therefore, PFC need gas cylinders to supply these gases for effective

power generation. This situation limits the design of compact enough PFC that can be accommodated in portable electronic devices.

Herein, we developed a PFC in which gas circulates internally. By circulating formed O_2 gas from the anode to the cathode, the reverse reaction at the anode could be prevented. The concept of gas-circulating PFC is shown in Figure 1a, Test 3. The PFC has two photocatalysts (TiO_2 and Ag- TiO_2) immersed in HCl solution. The electrolyte at the anode and that at the cathode (Fig. 1b2, 3) are separated by a PCP (Fig. 1b4, 5). As the mechanism of gas circulation, the PFC designed in this study comprises an organic solvent phase on an anode electrolyte (Fig. 1b1) and a vent hole in the upper part of the PCP film (Fig. 1b4, 5). The organic solvent can dissolve a greater amount of O_2 gas than water can.

O_2 gas circulated in the PFC as follows. O_2 generated by the anode reaction transferred preferentially into the organic solvent due to the difference in O_2 solubility between the HCl solution and the organic solvent. Then, the dissolved O_2 in the organic solvent moved to the upper gas phase due to the increased O_2 concentration in the solvent in the compartment of the anode, and then to the upper gas phase in the compartment of the cathode through the vent hole in the PCP film due to the pressure difference between the O_2 formed at the anode and O_2 consumed at the cathode (Fig. 1a, 1b1). Finally, the gaseous O_2 that moved to the cathode side reached the photocatalyst on the cathode and was photoreduced.

1 EXPERIMENTAL SECTION

1.1 Sample Preparation of the Photoelectrodes

TiO_2 powder [1.00 g; P25, Degussa; anatase/rutile phases = 7/3; Brunauer-Emmett-Teller (BET) surface area (S_{BET}) = 60 $\text{m}^2 \text{g}^{-1}$] was suspended in 3.0 mL of deionized water ($<0.06 \mu\text{S cm}^{-1}$) and then stirred well. The obtained suspension was dried at 373 K for 24 h and heated in air at 673 K for 2 h. The resultant powder was suspended in 75 μL of deionized water and placed on an Indium Tin Oxide (ITO, thickness 1.2-1.6 μm)-coated Pyrex glass plate. The TiO_2 /ITO/Pyrex was dried at 373 K for 18 h and heated in air at 573 K for 30 min. The amount of TiO_2 deposited on the ITO-coated glass plate was 5.0 mg and covered an area of 1.3 cm^2 .

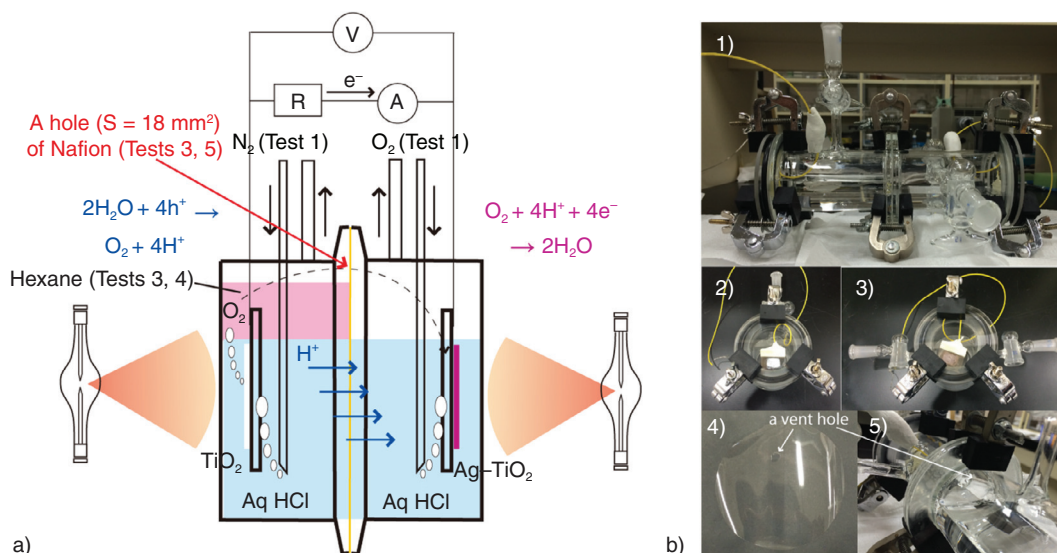


Figure 1

- a) Components of the PFC comprising TiO_2 and Ag-TiO_2 photocatalysts used for Tests 1-5. Oxidation by photogenerated holes at the anode and reduction by photogenerated electrons take place. Remaining electrons at the anode flow to the cathode and combine with the remaining holes.
- b) Photographs of the PFC for Test 3 (1). Photoanode side (2), photocathode side (3), and the PCP with a vent hole (4, 5).

Silver nitrate (159 mg; 99.8%, *Wako Pure Chemicals*) was dissolved in 10 mL of deionized water. The solution was mixed with 3.33 g of untreated TiO_2 (P25). The mixture was magnetically stirred at a rate of 850 rotations per minute (rpm) and the water was distilled at 353 K. The obtained powder was dried at 373 K for 24 h and heated in air at 673 K for 2 h. The resultant Ag-TiO_2 powders contained 3.0 wt% of Ag. They were suspended in a minimum amount of water and placed on ITO-coated glass ($\text{Ag-TiO}_2/\text{ITO}/\text{Pyrex}$) in a manner similar to that for the $\text{TiO}_2/\text{ITO}/\text{Pyrex}$.

1.2 Photocurrent Tests

1.2.1 Test 1: Gas-Flow Conditions

$\text{TiO}_2/\text{ITO}/\text{Pyrex}$ and $\text{Ag-TiO}_2/\text{ITO}/\text{Pyrex}$ electrodes were immersed in HCl solutions (40 mL in each compartment; initial pH 4.0-2.0). The two compartments were separated by a 50- μm -thick PCP film (Nafion, *DuPont*; acid capacity > 9.2×10^{-4} equivalent g^{-1}). N_2 (purity > 99.999%) and O_2 gases (purity > 99.6%) were bubbled 30 mm away from each photoelectrode at a flow rate of 100 mL min^{-1} (Fig. 1a). The PFC was equipped with quartz windows ($\phi = 80 \text{ mm}$) on both sides. Both the TiO_2 and Ag-TiO_2 photocatalysts were irradiated with UV-visible light through the quartz windows using a two-way branched quartz fiber light guide (Model 5 ϕ -2B-1000L, *San-ei Electric Co.*) from a 500-W xenon arc lamp (Model SX-UID502XAM, *Ushio*).

The distance between the light exit ($\phi = 5 \text{ mm}$) and the TiO_2 or Ag-TiO_2 film was 46 mm. The light intensity was 8 mW cm^{-2} at the center of the photocatalyst film on each electrode.

1.2.2 Test 2: Gas-Closed Conditions

PFC comprising $\text{TiO}_2/\text{ITO}/\text{Pyrex}$ and $\text{Ag-TiO}_2/\text{ITO}/\text{Pyrex}$ electrodes were prepared and immersed in HCl solutions (40 mL in each compartment; initial pH 2.0) in a similar procedure to that in Test 1. The two compartments were separated by a 50- μm -thick PCP film. N_2 and O_2 gases purged the compartments of $\text{TiO}_2/\text{ITO}/\text{Pyrex}$ and $\text{Ag-TiO}_2/\text{ITO}/\text{Pyrex}$, but the gas supply was stopped before the start of Test 2. Both the TiO_2 and Ag-TiO_2 photocatalysts were irradiated with UV-visible light in the closed compartments filled with N_2 and O_2 , respectively.

1.2.3 Test 3: Gas-Circulating Conditions inside the PFC

An $\text{Ag-TiO}_2/\text{ITO}/\text{Pyrex}$ electrode was immersed in 50 mL of HCl solution (initial pH 2.0), whilst $\text{TiO}_2/\text{ITO}/\text{Pyrex}$ was immersed in 50 mL of the HCl solution phase (initial pH 2.0) and 50 mL of hexane phase was added above the HCl solution phase (Fig. 1). All the area of the TiO_2 film was immersed in the HCl solution phase and not in contact with the hexane phase. N_2 and O_2 gases purged the compartments of $\text{TiO}_2/\text{ITO}/\text{Pyrex}$ and $\text{Ag-TiO}_2/\text{ITO}/\text{Pyrex}$,

TABLE 1
The conditions for current tests of the PFC

Test	N ₂ /O ₂ supply	Hexane@anode	Vent hole@PCP film
1	○	×	×
2	×	×	×
3	×	○	○
4	×	○	×
5	×	×	○

respectively, but the gas supply was stopped before the start of Test 3. Both the TiO₂ and Ag-TiO₂ photocatalysts were irradiated with UV–visible light, set in the closed compartments filled with N₂ and O₂, respectively. The two compartments were separated by a 50- μ m-thick PCP film; however, in Test 3, gas circulation inside the PFC was enabled through a vent hole (6.0 mm \times 3.0 mm) in the upper part of the PCP film (Fig. 1a, b4, b5) from the anode compartment in which O₂ was formed to the cathode compartment in which O₂ was consumed. The conditions of UV–visible light irradiation were similar to those for Tests 1 and 2 (Tab. 1).

1.2.4 Test 4: Gas-Closed Conditions Plus Hexane@Anode

An Ag-TiO₂/ITO/Pyrex electrode was immersed in 55 mL of HCl solution (initial pH 2.0), whilst TiO₂/ITO/Pyrex was immersed in 55 mL of the HCl solution phase (initial pH 2.0) and 55 mL of the hexane phase above the HCl solution phase (Fig. 1). All the area of the TiO₂ film was immersed in the HCl solution phase and not in contact with the hexane phase. N₂ and O₂ gases purged the compartments of TiO₂/ITO/Pyrex and Ag-TiO₂/ITO/Pyrex, respectively, but the gas supply was stopped before the start of Test 4. Both the TiO₂ and Ag-TiO₂ photocatalysts were irradiated with UV–visible light, set in the closed compartments filled with N₂ and O₂, respectively. The two compartments were separated by a 50- μ m-thick PCP film. The film was complete and did not comprise any vent holes as in Test 3. The conditions of UV–visible light irradiation were similar to those for Tests 1–3 (Tab. 1).

1.2.5 Test 5: Gas-Circulating Conditions inside the PFC Minus Hexane@Anode

An Ag-TiO₂/ITO/Pyrex electrode was immersed in 40 mL of HCl solution (initial pH 2.0), whilst TiO₂/ITO/Pyrex was immersed in 40 mL of the HCl solution phase (initial pH 2.0). N₂ and O₂ gases purged the compartments of TiO₂/ITO/Pyrex and Ag-TiO₂/ITO/Pyrex, respectively, but

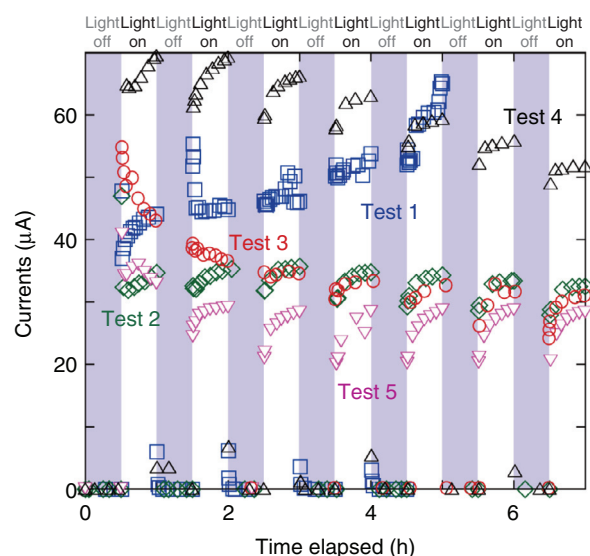


Figure 2

The time course of photocurrents of the PFC comprising TiO₂ and Ag-TiO₂ photocatalysts in Tests 1 (gas flow), 2 (gas closed), 3 (gas circulating inside the PFC), 4 (gas-closed conditions plus hexane@anode), and 5 (gas-circulating conditions inside the PFC minus hexane@anode). The pH values of the electrolytes in both the anode and cathode were 2.0.

the gas supply was stopped before the start of Test 5. Both the TiO₂ and Ag-TiO₂ photocatalysts were irradiated with UV–visible light, set in the closed compartments filled with N₂ and O₂, respectively. The two compartments were separated by a 50- μ m-thick PCP film. The conditions of UV–visible light irradiation were similar to those for Tests 1–4. This PFC had a vent hole (6.0 mm \times 3.0 mm) in the upper part of the PCP film (Fig. 1a, b4, b5) similar to Test 3 (Tab. 1).

For Tests 1–5, photocurrent generation (photocurrent tests) was performed by connecting the external parallel circuit for one route via a voltmeter and another route via an ammeter with a resistance of 0.5 Ω (Fig. 1a). Both catalysts were exposed for 30 min to UV–visible light and then kept in the dark for 30 min, and this process was repeated five–seven times. The current and voltage between the two electrodes were monitored.

1.3 Current–Voltage Dependence Tests

The current (i)–voltage (V) characteristics were also measured for several types of PFC using a similar parallel circuit (Fig. 1a). After the photocurrent test for Figure 2 (2.5, 3.5 and 3.5 h of irradiation of UV–visible light for Tests 1, 2 and 4, respectively), the resistance was gradually decreased from 500 k Ω to 0.3 Ω over 20 min to plot the i – V dependence. For comparison, a PFC in the conditions of Test 1

(Sect. 1.2.1) was also prepared and i - V characteristics were also measured similar to the experiments described above, but in darkness.

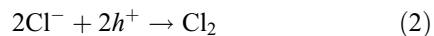
1.4 Product Analyses during Photocurrent Tests at the Anode

1.4.1 Analysis of O₂ Formed at the Anode

56.2 mg of iron(III) chloride hexahydrate (*Kanto Chemical*, purity $\geq 99\%$) was dissolved in 90 mL of HCl aqueous solution in a quartz flask. The pH of this solution was adjusted to 2.0 by the addition of HCl solution. 151 mg of TiO₂ powder (P25, *Degussa*) was suspended in this solution for 10 min. Then, dissolved O₂ in the solution was removed by N₂ bubbling for 30 min. Next, N₂ bubbling was stopped and the flask was isolated. The solution suspended with TiO₂ was irradiated with UV-visible light from model SX-UID502-XAM. The distance between the light exit ($\phi = 60$ mm) and the center of the flask was 120 mm. The sample was exposed to the light for 15 min and kept in the dark for 15 min. This step was repeated five times. The solution was magnetically stirred at a rate of 1 000 rpm and the temperature was 298-301 K. The formed O₂ as dissolved was monitored *in situ* by a Dissolved Oxygen (DO) electrode (Model 9520-10D, *Horiba*).

1.4.2 Analysis of Hypochlorous Acid Formed at the Anode by the Photooxidation of Cl⁻

The possibility of the photooxidation of Cl⁻ ions at the anode of the PFC instead of the photooxidation of water was checked. If Cl₂ is formed by the photooxidation at the anode (Eq. 2), it should immediately decompose into hypochlorous acid and hydrochloric acid in the HCl solution of the anode (Eq. 3):



The HClO formed was evaluated by the *N,N*-Diethyl-*p*-PhenyleneDiamine (DPD) method [22].

20 mg of DPD reagent (0.8 mg of DPD sulfate salt (H₂SO₄) and 19.2 mg of Na₂SO₄) were dissolved in 1.0 mL phosphate buffer solution (pH 6.5). This solution was mixed with 5.0 mL of 0-39.0 $\mu\text{mol L}^{-1}$ of NaOCl aqueous solutions and used as a standard solution. The mixed solutions (6.0 mL) were used to obtain a linear regression relationship between the absorbance at 515 nm and the concentration of ClO⁻ ions.

Next, 20 mg of DPD reagent were dissolved in 4.0 mL phosphate buffer solution (pH 6.5). This solution was mixed

with 2.0 mL of sample solution (HCl aqueous solution) after a photocurrent Test 1 using a PFC (Fig. 1) for 3 h at pH 2.0. The UV-visible spectrum of the mixed solution (6.0 mL) was measured by UV-visible spectrometer (Model V650, *JASCO*). The concentration of HClO in the sample was determined based on the absorbance at 515 nm and the relationship obtained using NaOCl standard solutions. The reason for the volume difference for the phosphate buffer and sample solutions was to adjust the pH within 6.4 and 6.6 for mixed solutions (6.0 mL).

2 RESULTS AND DISCUSSION

2.1 Photocurrent Tests

The time courses of the photocurrent tests are summarized in Figure 2. For Test 1, in response to the UV-visible irradiation, photocurrents gradually increased from 43.7 to 60.5 μA in five cycles at pH 2.0. In contrast, the photocurrents increased and converged to a constant value (26.7 μA) in the test at pH 3.0 (not shown) [11]. Thus, the active metallic Ag⁰ species for photoreduction of O₂ at the cathode should gradually increase, transformed from Ag₂O by the reaction with protons, in the five cycles at pH 2.0. The transformation of the active Ag species (Ag⁰, Ag₂O and AgCl) was reported based on an extended X-ray absorption fine-structure study [11].

At pH 4.0, a PFC current of 3 μA was obtained (not shown) for 2.5 h irradiated by UV-visible light (0.28 $\mu\text{mol-e}^-$ generated in total) [11]. The pH values starting from 4.0 for the HCl solution (40 mL, 4.0 $\mu\text{mol-H}^+$) remained constant after the PFC test at both the anode and cathode. The pH change due to each half reaction was calculated as ± 0.03 . As this value is nearly the accuracy of pH monitoring under these conditions, we cannot judge that the photooxidation of water (at the anode) and photoreduction of O₂ (at the cathode) exclusively took place. The possibility of a by-reaction, *e.g.* the consumption of acid, remained. For the test at pH 2.0, the initial proton concentration was 400 μmol in 40 mL of electrolyte solution at both the anode and cathode, while the PFC current for 2.5 h was 4.7 $\mu\text{mol-e}^-$ in total. The pH change due to each half reaction is calculated as ± 0.005 . It was even more difficult to judge the possibility of photooxidation of water and/or anions of acid under the conditions.

In Test 2, the photocurrent in the first cycle (34.7 μA) was similar to that in Test 1 (43.7 μA). In response to the UV-visible irradiation, photocurrents gradually increased to 35.8 μA in three cycles. In contrast to the gradual increase in photocurrents throughout 5 h of the study in Test 1, the photocurrents peaked at 35.8 μA in the third cycle and gradually decreased to 32.2 μA in the seventh cycle in Test 2 (Fig. 2). This decrease by 3.6 μA suggested partial

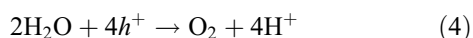
deactivation of the TiO₂ photocatalyst at the anode. One of the major reasons is the reverse reaction of produced O₂ which remained dissolved in the HCl solution to water (Eq. 1). In contrast to the gas-flowing Test 1, the anode compartment of TiO₂/ITO/Pyrex was purged with N₂ gas and produced O₂ remained in the compartment for Test 2 (Tab. 1).

The photocurrent in the first cycle (54.8–40.3 μA) was clearly higher in Test 3 than that in Tests 1 and 2. The photocurrent decreased to 36.5 μA at the end of the second cycle (Fig. 2) and continued to decrease gradually to 31.0 μA at the end of the seventh cycle. The photocurrents in the first cycle were probably higher because N₂ was purged in the anode compartment more completely than in Tests 1 and 2 by the effect of hexane to preferably dissolve a contamination level of O₂ (~0.04 ppb). This evaluation was based on the impurity of O₂ (< 1 ppm) in the N₂ gas used and the equilibrium of dissolution. Conversely, the decrease in the photocurrent in seven cycles suggested an even smaller amount of formed O₂ remained in the anode and inhibited the PFC performance considerably, and also unexpected reverse diffusion of O₂ from the cathode into the anode was not excluded through the vent hole.

In Test 4, the photocurrent in the first cycle (69.7 μA) was clearly higher than that in Tests 1–3. However, in response to the UV–visible irradiation, photocurrents gradually decreased to 51.9 μA in seven cycles (Fig. 2). The photocurrent in Test 4 was always higher than that in Tests 2 and 3 throughout the photocurrent test. Thus, the positive effects of hexane on PFC were confirmed (Tab. 1), but unexpectedly, the vent hole in Test 3 contributed negatively to the photocurrent generation. Furthermore, the linear decrease of the photocurrent as a function of time that elapsed during Test 4 was more gradual than the exponential-like decrease as a function of time in Test 3.

In Test 5, the photocurrent in the first cycle (41.0–33.0 μA) was similar to that in Test 2 (Fig. 2). Then, it decreased to 29.2 μA in the second cycle. Later than the third cycle, the photocurrents became stable at 28.4 μA. This stabilized current was lowest among the Tests 1–5, as the result of produced O₂ which remained dissolved in the HCl solution to water, and the unexpected reverse diffusion of O₂ in the cathode into the anode through the vent hole, as in Test 3 (Tab. 1).

In Test 2, 1.11 μmol of O₂ were generated during the 7-h photocurrent test based on the total photocurrent for 3.5 h and assuming the next reaction (Eq. 1 is the reverse reaction of Eq. 4):



All of them were dissolved in the anode electrolyte based on the O₂ solubility. Thus, the O₂ concentration in the anode electrolyte was 27.8 μmol L⁻¹. On the other hand, in Test 4, 2.01 μmol of O₂ were generated after the 7-h photocurrent

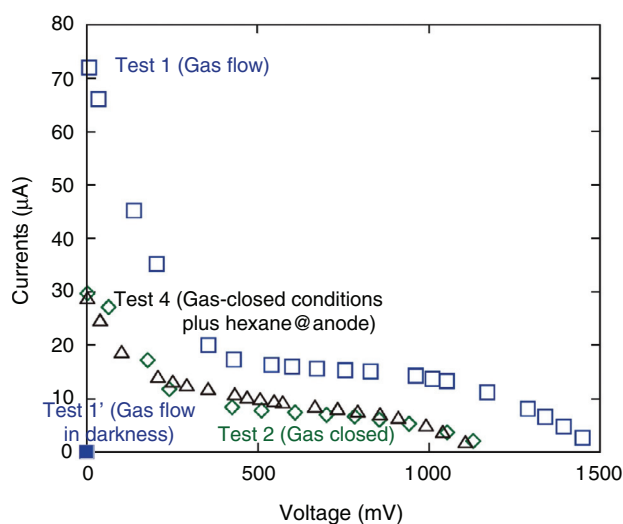


Figure 3

i-*V* characteristics of the PFC comprising TiO₂ and Ag-TiO₂ photocatalysts in Test 1 (gas flow), Test 2 (gas closed), Test 4 (gas-closed conditions plus hexane@anode), and control Test 1' in darkness (gas flow).

test based on the total photocurrent for 3.5 h and assuming reaction 4. In this test, the O₂ should be distributed between the HCl solution and hexane. Based on the O₂ solubility values in the literature to hydrochloric acid solution (1.27 mmol L⁻¹) and to hexane (15.0 mmol L⁻¹) [23], the distribution of O₂ to hexane was calculated as:

$$\frac{0.055 \text{ L} \times 15 \text{ mmol L}^{-1}}{0.055 \text{ L} \times 1.27 \text{ mmol L}^{-1} + 0.055 \text{ L} \times 15 \text{ mmol L}^{-1}} = 0.922 \quad (5)$$

Thus, 1.85 and 0.157 μmol of O₂ should be distributed to the hexane and HCl solutions, respectively, in equilibrium. Thus, the O₂ concentration in the anode electrolyte (HCl solution) was calculated as 2.85 μmol L⁻¹. Hence, the O₂ concentration at the end of Test 4 was only 10% of that at the end of Test 2. This difference accounted for the higher current density in Test 4 by a factor of two as compared with Test 2 (Fig. 2).

2.2 *i*-*V* Characteristic Tests

The obtained *i*-*V* characteristics are shown in Figure 3. Furthermore, the properties of PFC calculated based on *i*-*V* data in Tests 1, 2 and 4 are summarized in Table 2. In Test 1, the *i* value gradually increased as the cell voltage decreased, starting from open circuit voltage (*V*_{OC}) at 1.59 V, which is a similar trend to the *i*-*V* dependence of the SC [24] or the Ohmic

TABLE 2
PFC characteristics defined by i - V characteristics in Tests 1 (gas flow), 2 (gas closed), and 3 (gas circulating inside the PFC)

Test	I_{SC} (μ A)	V_{OC} (V)	P_{Max} (μ W)
1 (Gas flow)	73.7	1.59	14.0
2 (Gas closed)	29.8	1.23	5.5
4 (Gas-closed conditions plus hexane@anode)	29.2	1.18	6.1
1' (Gas flow; control in darkness)	< 0.1	< 0.002	< 0.0002

loss region of a Polymer Electrolyte Fuel Cell (PEFC). When the voltage became less than 0.45 V, the current increased linearly from 20 to 74 μ A (short-circuit current, I_{SC}). This increasing trend was different from that in a SC or the transportation limit region of a PEFC [7, 8].

In Test 2, the shape of the i - V characteristic curve was similar to that for Test 1. However, the increase in currents in the lower voltage region (≥ 0.45 V) was less steep than the slope in Test 1. The values of I_{SC} (29.8 μ A), V_{OC} (1.23 V) and P_{Max} (5.51 μ W) were 40, 77 and 39% of the corresponding values obtained in Test 1. The lower photocurrents in Test 2 suggested that the reverse reaction 1 that occurred in the anode seriously affected the performance of the PFC.

In Test 4, the curve of i - V characteristics was similar to that for Test 2; the increase in photocurrents in the low-voltage region (≥ 0.45 V) was less steep than the slope in Test 1. The values of I_{SC} (29.2 μ A) and V_{OC} (1.18 V) were slightly lower than the corresponding values in Test 2, whilst the value of P_{Max} (6.10 μ W) was clearly higher than that in Test 2 (5.51 μ W). This low performance (Fig. 3) was inconsistent with the better performance in photocurrent Test 4 than that in Tests 1 and 2 (Fig. 2). This trend cannot be rationalized based on the remaining amount of produced O_2 dissolved in the anode. One of the possibilities is the polarization of photoelectrodes during the i - V measurements at high voltage to modify the band bending (charge balance at the surface) at the surface of photocatalysts [25-29].

In a control Test 1' in darkness, the value of the current was always less than the detection limit by changing the resistance from 500 k Ω to 0.3 Ω . The corresponding voltage was less than 0.002 V. Therefore, the values of I_{SC} , V_{OC} and P_{Max} were less than 0.1 μ A, 0.002 V and 0.0002 μ W, respectively. This indicated electricity of the PFC was generated exclusively by irradiation with UV-visible light.

2.3 Product Analyses during Photocurrent Tests at the Anode

2.3.1 Analysis of O_2 Formed at the Anode

The time course of dissolved O_2 concentrations is shown in Figure 4. When TiO_2 was irradiated with UV-visible light,

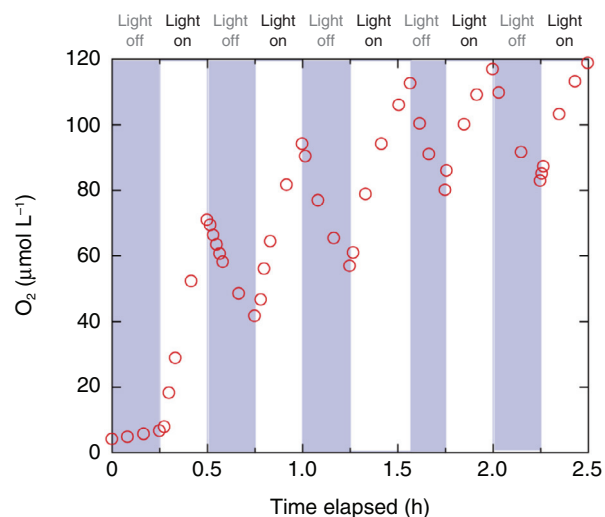


Figure 4

The time course of dissolved O_2 concentrations during the photoirradiation test on TiO_2 . UV-visible light and $FeCl_3 \cdot 6H_2O$ (2.31 mmol L^{-1}) were used as excitation light and a sacrificial reagent, respectively. The initial pH value was 2.0.

the dissolved O_2 concentration linearly increased immediately in all five cycles. For 1.25 h irradiation, dissolved O_2 was increased from 7.8 μ mol L^{-1} to 119 μ mol L^{-1} . If the irradiation was stopped, dissolved O_2 decreased gradually in all cycles. This indicated that the formed O_2 dissolved in acidic water and was transported to the gas phase in the quartz flask. In this photoreaction test, 151 mg of TiO_2 was used, significantly greater than the 5 mg for the photocurrent test (Sect. 2.1, 2.2). Accordingly, a greater amount of O_2 was generated from the water (63.1 μ mol L^{-1} per 0.25 h) in this photoreaction test than in photocurrent Test 2 (27.8 μ mol L^{-1} per 3.5 h). Thus, excessive O_2 greater than the dissolution amount would be transported to the gas phase.

When the photocatalyst was irradiated, the rate would be the balance between O_2 formation and the transportation to

the gas phase. The increase in dissolved O₂ in the first cycle was the quickest among all the cycles. The increase in dissolved O₂ was 63.1 μmol L⁻¹ per 0.25 h. The slope of the dissolved O₂ gradually became less steep as the cycles were repeated. As a result, in the fifth cycle, it was 36.2 μmol L⁻¹ per 0.25 h. This trend is contradicted by the gradual increase in the photocurrent in Figure 2, Test 1 as the cycles repeated. We suspect that the major reason was that the transportation of dissolved O₂ to the gas phase became faster as the concentration of dissolved O₂ increased, as the cycles were repeated (Fig. 4).

The increase rate of dissolved O₂ in the first cycle was:

$$63.1 \mu\text{mol L}^{-1} \times 0.090 \text{ L}/0.25 \text{ h}/0.151 \text{ g}_{\text{cat}} = 151 \mu\text{mol-O}_2 \text{ h}^{-1} \text{ g}_{\text{cat}}^{-1} \quad (6)$$

In comparison, the total photocurrent in Test 2 was average current:

$$34.0 \mu\text{A} \times 3600 \text{ s h}^{-1}/9.65 \times 10^4 \text{ A s mol-e}^{-1}/0.0050 \text{ g}_{\text{cat}} = 253 \mu\text{mol-e}^{-1} \text{ h}^{-1} \text{ g}_{\text{cat}}^{-1} \quad (7)$$

The electron flow rate corresponded to the O₂ generation rate of 63 μmol-O₂ h⁻¹ g_{cat}⁻¹. The net O₂ generation rate in Figure 4 should be even higher because the O₂ transported to the gas phase was not included for the evaluation in Figure 4. This difference in the amount based on the PFC current was not inconsistent. In the presence of a sacrificial oxidation agent, Fe³⁺, photoexcited electrons to the conduction band of TiO₂ easily diffuse with sufficient Fe³⁺ and react in contrast so that the electrons need to travel to the cathode to react with holes at the valence band of [Ag-]TiO₂ in the PFC. The concentration of holes was determined by the balance of charge separation by light and the cathode reaction rate of O₂ reduction [11, 21].

2.3.2 Analysis of Hypochlorous Acid Formed at the Anode from Cl⁻ Ions

The absorbance at 515 nm for standard mixed solutions (6.0 mL) was plotted as a function of NaOCl concentrations in the solution (6.0 mL). Then, a standard curve was calculated as follows (Fig. 5):

$$\text{Absorbance}@515 \text{ nm} = 0.0166 \times [\text{ClO}^-] (\mu\text{mol L}^{-1}) + 0.007 \quad (8)$$

20 mg of DPD reagent in 4.0 mL phosphate buffer solution (pH 6.5) were mixed with 2.0 mL of sampled solution from the anode solution (40 mL) of the PFC after Test 1 for 3 h. The absorbance of this mixed solution was 0.018 ± 0.008. Therefore, the amount of HClO in the mixed solution (6.0 mL) was 3.98 nmol based in Equation (8).

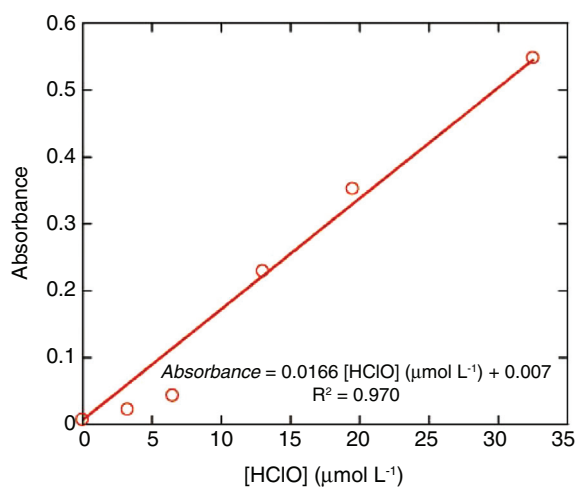


Figure 5

Absorbance at 515 nm for standard mixed solutions as a function of the concentration of HClO standard solutions.

Thus, the amount of HClO in the anode solution was calculated as:

$$3.98 \text{ nmol} \times 40 \text{ mL}/2.0 \text{ mL} = 0.080 \pm 0.056 \mu\text{mol} \quad (9)$$

For 3 h of Test 1 (pH 2.0), total electron flow was 3.92 μmol based on the integration of photocurrents. Two holes reacted with Cl⁻ ions (Eq. 2) correspond to one HClO formed from Cl₂ (Eq. 3). As the concentration of HClO was the impurity level for the anode solution in Test 1, the amount of HClO was nearly the detection limit. Therefore, the upper limit of selectivity to proceed with Equation (2) for photogenerated holes was:

$$2 \times 0.080 \mu\text{mol-HClO}/3.92 \mu\text{mol-h}^+ = 0.041 \pm 0.031 \quad (10)$$

The participation of chlorine ions in the anode reaction cannot be denied; however, the ratio was as low as 4.1% at most.

CONCLUSIONS

First, the anode reaction in the PFC was demonstrated exclusively to be the photooxidation of water over TiO₂ based on the O₂ evolution test, and negligible (or no) photooxidation of Cl⁻ occurred based on the detected amount of HClO. The selectivity of photooxidation of Cl⁻ was 4.1% at most as compared with the photooxidation of water. Next, a product gas-trapping PFC was demonstrated to achieve a

photocurrent value of 69.7 μA per 1.3 cm^2 of photocatalysts (53.6 $\mu\text{A cm}^{-2}$). Gas trapping was enabled by accommodating an organic solvent layer over the aqueous electrolyte solution phase in the anode and utilizing the solubility difference of produced O_2 . However, gas circulation by a vent hole in the upper part of the PCP film due to pressure differences was not well achieved. To transfer generated O_2 to an anode, a greater pressure difference was needed. The performance of the gas-closed PFC equipped with a hexane layer on the anode (Test 4) was the best at the initial stage of the photocurrent test due to the O_2 solubility effect of hexane rather than the other conditions. However, the photocurrents gradually decreased during the measurements for 7 h. The small amount of remaining O_2 in the anode electrolyte (2.85 $\mu\text{mol L}^{-1}$) reduced the PFC performance considerably in Test 4. The I_{SC} , V_{OC} and P_{Max} values of the gas-circulating PFC were 29.2 μA (22.5 $\mu\text{A cm}^{-2}$), 1.18 V and 6.10 μW (4.69 $\mu\text{W cm}^{-2}$), respectively. These values were similar to corresponding values for the gas-closed PFC.

The feasibility of a gas-trapping PFC was successfully demonstrated in this study. Further, the improvement of power efficiency is required by the optimization of photocatalysts and the thickness and density of photocatalyst layers in order to be accommodated in portable electronic devices, remote-control light gliders, and environmental cameras/sensors.

ACKNOWLEDGMENTS

The authors are grateful for financial support from the Feasibility Study Stage of A-STEP (AS262Z00159L, AS251Z00906L, AS231Z01459C) from the Japan Science and Technology Agency, the Iwatani Naoji Foundation (2011-2012), and a Grant-in-Aid for Scientific Research C (26410204, 22550117) from the Japan Society for the Promotion of Science. X-ray absorption experiments were conducted under the approval of the Photon Factory Proposal Review Committee (2013G159).

REFERENCES

- Lewis N.S., Nocera D.G. (2006) Powering the Planet: Chemical Challenges in Solar Energy Utilization, *Proc. Natl. Acad. Sci. USA* **103**, 15729.
- Izumi Y. (2013) Recent Advances in the Photocatalytic Conversion of Carbon Dioxide to Fuels with Water and/or Hydrogen Using Solar Energy and Beyond, *Coord. Chem. Rev.* **257**, 171.
- Bolton J.R. (1996) Solar Photoproduction of Hydrogen: A review, *Sol. Energy* **57**, 37.
- Grätzel M. (2001) Photoelectrochemical Cells, *Nature* **414**, 338.
- Gasteiger H.A., Marković N.M. (2009) Just a Dream or Future Reality? *Science* **324**, 48.
- Schlapbach L. (2009) Hydrogen-Fuelled Vehicles, *Nature* **460**, 809.
- Oka K., Ogura Y., Izumi Y. (2014) X-Ray Evaluation of the Boundary between Polymer Electrolyte and Platinum and Carbon Functionalization to Conduct Protons in Polymer Electrolyte Fuel Cell, *J. Power Sources* **258**, 83.
- Oka K., Shibata Y., Itoi T., Izumi Y. (2010) Synthesis and Site Structure of a Replica Platinum–Carbon Composite Formed Utilizing Ordered Mesopores of Aluminum-MCM-41 for Catalysis in Fuel Cells, *J. Phys. Chem. C* **114**, 1260.
- Joya K.S., Joya Y.F., Ocakoglu K., van de Krol R. (2013) Water-Splitting Catalysis and Solar Fuel Devices: Artificial Leaves on the Move, *Angew. Chem. Int. Ed.* **52**, 10426.
- Seery M.K., George R., Floris P., Pillai S.C. (2007) Silver Doped Titanium Dioxide Nanomaterials for Enhanced Visible Light Photocatalysis, *J. Photochem. Photobiol. A* **189**, 258.
- Ogura Y., Okamoto S., Itoi T., Fujishima Y., Yoshida Y., Izumi Y. (2014) A photofuel Cell Comprising Titanium Oxide and Silver(I/O) Photocatalysts for Use of Acidic Water as a Fuel, *Chem. Comm.* **50**, 3067-3070.
- Huang S.Y., Ganesan P., Park S., Popov B.N. (2009) Development of a Titanium Dioxide-Supported Platinum Catalyst with Ultrahigh Stability for Polymer Electrolyte Membrane Fuel Cell Applications, *J. Am. Chem. Soc.* **131**, 13898.
- Orilall M.C., Matsumoto F., Zhou Q., Sai H., Abruna H.D., DiSalvo F.J., Wiesner U. (2009) One-Pot Synthesis of Platinum-Based Nanoparticles Incorporate into Mesoporous Niobium Oxide–Carbon Composites for Fuel Cell Electrodes, *J. Am. Chem. Soc.* **131**, 9389.
- Sun Y., Zhuang L., Lu J., Hong X., Liu P. (2007) Collapse in Crystalline Structure and Decline in Catalytic Activity of Pt Nanoparticles on Reducing Particle Size to 1 nm, *J. Am. Chem. Soc.* **129**, 15465.
- Wang L.L., Johnson D.D. (2007) Shear Instabilities in Metallic Nanoparticles: Hydrogen-Stabilized Structure on Pt₃₇ on Carbon, *J. Am. Chem. Soc.* **129**, 3658.
- Izumi Y., Nagamori H., Kiyotaki F., Masih D., Minato T., Roisin E., Candy J.P., Tanida H., Uruga T. (2005) X-ray Absorption Fine Structure Combined with X-ray Fluorescence Spectrometry. Improvement of Spectral Resolution at the Absorption Edges of 9–29 keV, *Anal. Chem.* **77**, 6969.
- Hanna M.C., Nozik A.J. (2006) Solar Conversion Efficiency of Photovoltaic and Photoelectrolysis Cells with Carrier Multiplication Absorbers, *J. Appl. Phys.* **100**, 074510.
- Morikawa M., Ogura Y., Ahmed N., Kawamura S., Mikami G., Okamoto S., Izumi Y. (2014) Photocatalytic Conversion of Carbon Dioxide into Methanol in Reverse Fuel Cells with Tungsten Oxide and Layered Double Hydroxide Photocatalysts for Solar Fuel Generation, *Catal. Sci. Technol.* **4**, 1644.
- Heller A. (1981) Conversion of Sunlight into Electrical Power and Photoassisted Electrolysis of Water in Photoelectrochemical Cells, *Acc. Chem. Resear.* **14**, 154.
- Chen F., Liu H., Bagwasi S., Shen X., Zhang J. (2010) Visible-Light Responsive Photocatalytic Fuel Cell Based on WO₃/W Photoanode and Cu₂O/Cu Photocathode for Simultaneous Wastewater Treatment and Electricity Generation, *Environ. Sci. Technol.* **46**, 11451.

- 21 Fujishima Y., Okamoto S., Yoshida Y., Itoi T., Kawamura S., Yoshida Y., Ogura Y., Izumi Y. (2015) Photofuel Cell Comprising Titanium Oxide and Bismuth Oxychloride ($\text{BiO}_{1-x}\text{Cl}_{1-y}$) Photocatalysts for Use of Acidic Water as a Fuel, *J. Mater. Chem. A* **3**, 8389.
- 22 Moberg L., Karlberg B. (2000) An Improved *N,N'*-Diethyl-*p*-Phenylenediamine (DPD) Method for the Determination of Free Chlorine Based on Multiple Wavelength Detection, *Anal. Chim. Acta* **407**, 127.
- 23 Battino R., Rettich T.R., Tominaga T. (1983) The Solubility of Oxygen and Ozone in Liquids, *J. Phys. Chem. Ref. Data* **12**, 163.
- 24 Anderson A.Y., Barnes P.R.F., Durrant J.R., O'Regan B.C. (2011) Quantifying Regeneration in Dye-Sensitized Solar Cells, *J. Phys. Chem. C* **115**, 2439.
- 25 Hu Z.T., Liu J., Yan X., Oh W.D., Lim T.T. (2015) Low-Temperature Synthesis of Grapheme/ $\text{Bi}_2\text{Fe}_4\text{O}_9$ Composite for Synergistic Adsorption-Photocatalytic Degradation of Hydrophobic Pollutant under Solar Irradiation, *Chem. Eng. J.* **262**, 1022.
- 26 Wu W., Huang Z.H., Lim T.T. (2014) Recent Development of Mixed Metal Oxide Anodes for Electrochemical Oxidation of Organic Pollutants in Water, *Appl. Catal. A* **480**, 58.
- 27 Nath R.K., Zain M.F.M., Kadhum A.A.H. (2014) Artificial Photosynthesis using LiNbO_3 as Photocatalyst for Sustainable and Environmental Friendly Construction and Reduction of Global Warming: A Review, *Catal. Rev. Sci. Eng.* **56**, 175.
- 28 Swierk J.R., Mallouk T.E. (2013) Design and Development of Photoanodes for Water-Splitting Dye-Sensitized Photoelectrochemical Cells, *Chem. Soc. Rev.* **42**, 2357.
- 29 Wenyi T., Qin Z., Han Y., Xiufang Z., Hongyi L. (2012) Deactivation Anode Catalyst $\text{La}_{0.75}\text{Sr}_{0.25}\text{Cr}_{0.5}\text{Mn}_{0.5}\text{O}_{3+\delta}$ in SOFC with Fuel Containing Hydrogen Sulfur: The Role of Lattice Oxygen, *Int. J. Hydrogen Energy* **37**, 7398.

Manuscript submitted in October 2014

Manuscript accepted in September 2015

Published online in October 2015